공학석사 학위논문

Design and synthesis of small-molecules and polymers based on extended isoindigo for organic solar cells

유기 태양 전지를 위한

확장된 아이소인디고 기반 단분자와 고분자의

설계 및 합성

2015년 8월

서울대학교 대학원

재료공학부

안 광 현

Abstract

Design and synthesis of small-molecules and polymers based on extended isoindigo for organic solar cells

An, Kwanghyeon

Department of Materials Science and Engineering

Seoul National University

New small molecules and conjugated copolymers based on extended isoindigo (eI) and oligothiophene (nT) were synthesized (eI-$(T)_2$, eI-$(2T)_2$, PeI-1T and PeI-3T) to investigate the photovoltaic properties of extended isoindigo unit. Extended isoindigo can be synthesized from two oxindoles and 2,2′-bithiophene-5,5′-dicarbaldehyde by a simple Knoevenagel condensation. Extended isoindigo shows weaker electron-accepting ability than isoindigo. Therefore the small molecules and copolymers based on extended isoindigo show up-shifted LUMO levels as compared to conventional isoindigo-based materials. Also extended isoindigo-based polymers exhibit a good π-π stacking due to perfectly planar structure of eI. The photovoltaic devices based on PeI-1T blended with $PC_{61}BM$ exhibits power conversion efficiency (PCE) of 4.07% with a J_{SC} of 11.86 mA cm^{-2}. Extended isoindigo could be a promising building block for efficient organic solar cells.

Keywords: extended isoindgo, small molecule, conjugated copolymer, Knoevenagel condensation, organic solar cells

Student Number: 2013-23820

Contents

List of Schemes

List of Figures

List of Tables

1. Introduction

Harvesting solar energy using solution-processed bulk-heterojunction (BHJ) organic photovoltaic (OPV) is considered as one of the attractive ways to satisfy the future global need for renewable energy sources due to the immense potential, such as easy fabrication, low production cost, light weight and flexibility of organic molecules, compared to inorganic solar cell.[1,2] Solution-processed BHJ organic solar cells based on blends of conjugated organic materials and fullerene derivatives have been extensively studied for highly efficient photovoltaics since first reported in 1995 with 2.9% power conversion efficiency (PCE).[3,4] The dramatic development of performance of BHJ OPVs has been achieved over the past few years benefited from the photoactive material design, morphology control and device optimization.[5,6] Through such an effort, PCEs of BHJ OPVs have surpassed 9% for single-layer solar cells[7] and 11% for tandem solar cells[8,9].

The general mechanism of electrical power generation requires four steps:[3,28] (1) absorption of photon by the photoactive material. The breakthrough of power conversion efficiency in a short period time may be attributed from the concept of donor (D)-acceptor (A) type low-band-gap organic solar cell. Low bandgap conjugated organic materials could be possible to absorb long-range wavelength of solar energy and produce more excitons in the active layer[10]; (2) a diffusion of generated exciton to the interface between donor and acceptor in the photoactive layer. To satisfy the condition, donor and acceptor material should be well-mixed and construct

interpenetrated network. Exciton could diffuse in the range of 10~20nm. So domain sizes of donor and acceptor material need to be small enough to achieve high performance solar cell[11]; (3) charge separation into electron and hole at the D/A interface.[12] Driving force for charge separation is related with difference between lowest unoccupied molecular orbital (LUMO) energy levels of donor and acceptor, known for 0.3 eV, called LUMO energy level offset[2,13]; (4) charge transport and collection.[14] On this step, charge mobility is important factor which is related with crystallinity of donor and blend morphology.

Based on understanding of power generation process, there have been five key points for designing semiconducting p-type materials of highly efficient BHJ solar cells: (1) a low bandgap and strong absorption for efficient photon harvesting in visible region of solar spectrum, leading to higher photocurrents; (2) a suitable highest occupied molecular orbital (HOMO) energy level for high open-circuit voltage (V_{OC}) and a proper lowest unoccupied molecular orbital (LUMO) energy level for efficient exciton dissociation at the interface between donor and acceptor; (3) high charge-carrier mobility to enhance charge transport efficiency which is related with the fill factor (FF); (4) optimal morphology; and (5) high solubility and stability.[15,16]

Design on donor-acceptor (D-A) type alternating copolymers and A-D-A(or D-A-D) type small-molecules have been proved to be a powerful strategy to develop low bandgap donor materials for efficient BHJ solar cells. The advantage of this class of conjugated materials is not only broad

absorption spectra but also easily tuned energy levels by combining different electron-donating units and electron-accepting units.[17]

Isoindigo (I), a structure isomer of pigment indigo, is strongly electon-deficient unit resulting from its two lactam rings. Reynolds *et al*. first reported isoindigo-based small-molecules for organic solar cells.[18] After that, isoindigo was recognized as ideal electron-deficient building block for D-A type conjugated polymers for BHJ OPVs due to its strong π−π interaction and excellent light absorption property as well as strong electron-withdrawing ability.[19-21] For these advantages, a variety of isoindigo-based small-molecules and polymers for BHJ solar cells have been intensively investigated in the past years.[22,23,31] To date, the best isoindigo-based OPVs exhibited a PCE beyond 7% for conventional cells and 8% for inverted cells.[24-25] However, isoindigo has some drawbacks. Because of strong electron-withdrawing ability, isoindigo-based materials have low-lying LUMO energy levels. It could be a detrimental effect on charge separation efficiency at the D/A interface Moreover, It is beneficial to directly connect five membered rings, such as thiophene and selenophene, to isoindigo unit since they could make planar backbone and promote intermolecular interaction. On the other hand, direct connection of six membered rings, most representatively benzene, with isoindigo unit has negative effects on photovoltaic performances.[26]

For these reasons, extended isoindigo (eI)[27,32,33], modified isoindigo by incorporating 2,2'-bithiophene in the middle of isoindigo unit, was synthesized to enlarge LUMO energy offset of isoindigo-based materials for

ensuring efficient exciton dissociation and was coupled with oligothiophene (nT).[29,30] In order to investigate the influence of changing electon-deficient unit from isoindigo to extended isoindigo in terms of energy levels and geometry, density functional theory (DFT) calculation was carried out at the B3LYP/6-31G (d, p) level on the isoindigo and extended isoindigo. Extended isoindigo shows up-shifted LUMO level compared to the isoindigo and even isoindigo flanked by thiophene. This result supports that extended isoindigo is weaker electron-accepting unit than isoindigo resulting from incorporating electron-rich unit, 2,2′-bithiophene. Furthermore, the geometry optimization of eI and I shows that extended isoindigo has a perfectly planar structure while isoindigo unit shows a slight torsion (13.9° angle) between the two oxindole rings along the central double bond. This is because the steric repulsion between oxygen atoms of oxindoles and protons of benzene moieties was disappeared and favorable (thienyl)S...O(carbonyl) nonbonding interactions was created.[34] Consequently, extended isoindigo-based materials would demonstrate a planar structure and good intermolecular packing which promote the high charge mobility. In this study, extended isoindigo-based donor materials (i.e., eI-$(T)_2$, eI-$(2T)_2$, PeI-1T and PeI-3T) was synthesized with eI and nT to investigate photovoltaic properties of extended isoindigo-based conjugated material as donor for BHJ organic solar cells. The optical, electrochemical and charge transport properties of donor materials are examined. Also morphological study of donor materials/$PC_{61}BM$ blend was performed to understand the performance of organic solar cells based on extended isoindgo-based materials.

2. Experimental Section

2.1. Materials

All reagents were purchased from Sigma-Aldrich, Alfa-Aesar, TCI chemicals, and Acros Organics and used as received. Tetrahydrofuran (THF) (Samchun pure chemicals) was dried over sodium/benzophenone and freshly distilled before use. Anhydrous toluene and N,N-dimethylformamide (DMF) was also purchased from Samchun pure chemicals and freshly purified by solvent purifier (PS-Micro, Innovative technology). Also, all solvent used for Stille coupling was bubbled with argon gas for 15 minutes before use. [6,6]-phenyl-C_{61}-butyric acid methyl ester ($PC_{61}BM$) was obtained from Nano-C and poly(3,4-ethylenedioxythiophene):poly(styrene sulfonate) (PEDOT:PSS) (Clevios P VP AI 4083) was purchased from H.C. Stark.

2.2. Synthesis of small-molecules

Extended isoindigo-based small-molecules, (3Z,3′Z)-3,3′-(2,2′-bithiophene-5,5′-diylbis(methan-1-yl-1-ylidene))bis(1-(2-ethylhexyl)-6-(5-hexyl-thiophen-2-yl)-indolin-2-one) (eI-$(T)_2$) and (3Z,3′Z)-3,3′-(2,2′-bithiophene-5,5′-diylbis(methan-1-yl-1-ylidene))bis(1-(2-ethylhexyl)-6-(5'-hexyl-[2,2']bithiophenyl-5-yl)-indolin-2-one) (eI-$(2T)_2$), were synthesized via Stille coupling between dibrominated eI (3) and monostannylated electron-donating units (5 and 7).

2.2.1. Synthesis of 2,2′-bithiophene-5,5′-dicarbaldehyde (1)

n-butyllithium (n-BuLi) (2.5M in hexane, 21.2 ml, 0.052 mol) was added dropwise to a solution of 2,2′-bithiophene (4 g, 0.024 mol) in

anhydrous THF (100mL) at −78℃, which was bubbled with argon gas. After the addition of n-BuLi, the mixture was stirred at r.t. for 1 h and then cooled to −78 ℃. After cooling, anhydrous DMF (9.3mL, 0.120 mol) was added dropwise to this solution at −78 ℃. The mixture was stirred at −78 ℃ for another 1 h and then warmed to r. t. slowly. After stirring at r. t. for 2 h, the mixture was poured into cool water (200mL). Yellow solid was precipitated. A further purification procedure by chromatography on silica gel (THF as eluent) was needed. After all, recrystallization from THF and hexane gave yellow solid. (2.07 g, 39%) ^{1}H NMR (300 MHz, $CDCl_3$, δ): 9.92 (s, 2H), 7.72 (d, 2H), 7.42 (d, 2H). ^{13}C NMR (125 MHz, $CDCl_3$, δ): 182.77, 145.05, 144.09, 137.28, 126.70.

2.2.2. Synthesis of (3Z,3′Z)-3,3′-(2,2′-bithiophene-5,5′-diylbis-(methan-1-yl-1-ylidene))bis(6-bromoindolin-2-one) (2)

To a suspension of 6-bromooxindole (2.20 g, 10.0 mmol) and 2,2′-bithiophene-5,5′-dicarbaldehyde (1.10 g, 5.0 mmol) in ethanol (35 mL), piperidine (0.5 mL) was added. The mixture was refluxed for 24 h and a red precipitate formed. The reaction mixture was cooled to room temperature and was filtered. The solid material was washed with ethanol and was dried under vacuum to give the compound 2 (2.60 g, 85%). Due to its poor solubility, the product was used for the next step directly without further characterization.

2.2.3. Synthesis of (3Z,3′Z)-3,3′-(2,2′-bithiophene-5,5′-diylbis-(methan-1-yl-1-ylidene))bis(6-bromo-1-(2-ethylhexyl)indolin-2-one) (3)

Anhydrous potassium carbonate (227 mg, 1.64 mmol) and compound 2 (200 mg, 0.33 mmol) were dissolved in anhydrous DMF (8 mL) bubbled with argon for 20 minutes. The solution was heated at 120 ℃ for 1 h under argon. 2-ethylhexylbromide (189 mg, 0.98 mmol) was added dropwise and the mixture was heated at 120 ℃ for 24 h. It was cooled to room temperature and was poured into water (300 mL). The mixture was extracted with dichloromethane. The combined organic layer was collected and was dried with $MgSO_4$. The solvent was removed under reduced pressure and the residue was purified by silica chromatography with eluent (CH_2Cl_2: hexane = 2:1) to give compound 3. (120 mg, 44%) ^{1}H NMR (300 MHz, $CDCl_3$, δ): 7.67 (d, 2H), 7.64 (s, 2H), 7.47 (d, 2H), 7.38 (d, 2H), 7.19 (d, 2H), 6.98 (s, 2H), 3.69 (d, 4H), 1.90 (m, 2H), 1.44–1.30 (m, 16H), 0.96–0.83 (m, 12H).

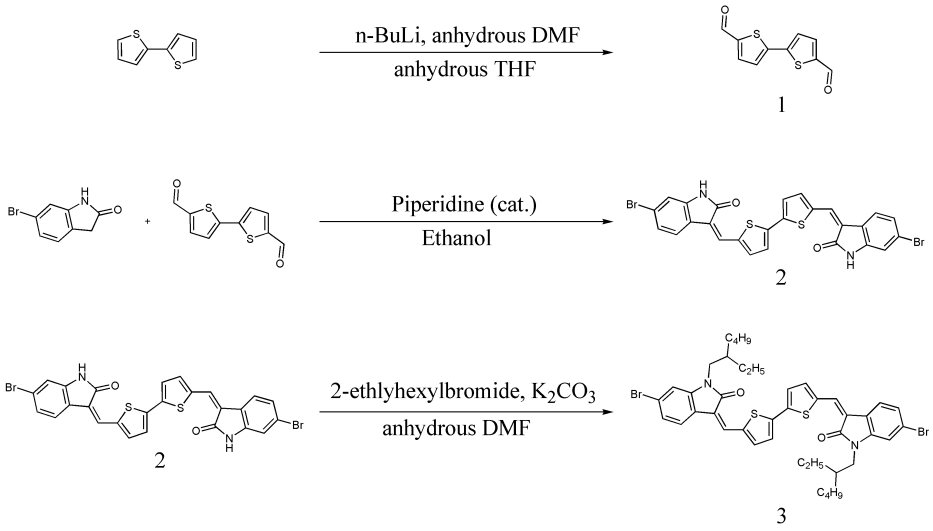

Scheme 2.1 The synthetic scheme of extended isoindigo and its alkylation.

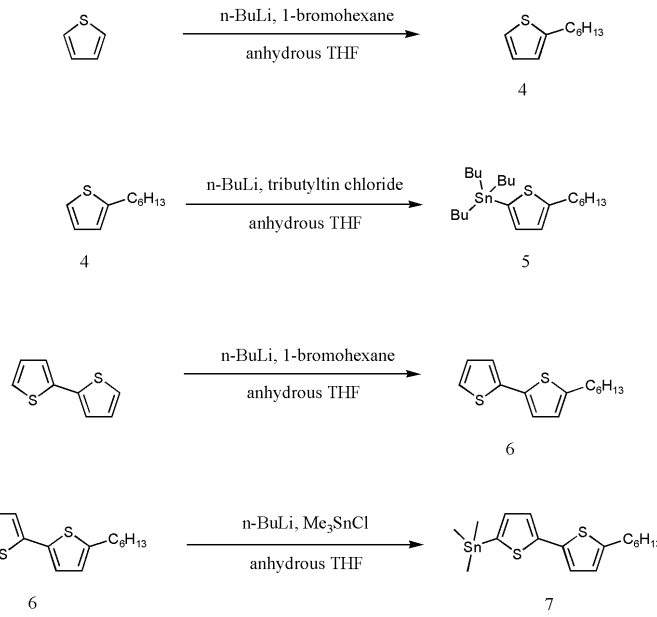

Scheme 2.2 The synthetic scheme of electron-rich units of small-molecules

2.2.4. Synthesis of 2-hexylthiophene (4)

To a solution of thiophene (2.33 g, 27.7 mmol) in 50 mL of dry THF, n-butyllithium (2.5 M in hexane) (10.7 ml, 27.7 mmol) was added dropwisely at −78 °C under a Ar atmosphere and kept stirring for 1 h. Then 1-bromohexane (5.03 g, 30.5 mmol) was added in one portion and the solution was warm to room temperature. After 15 h, the solution was purged into cold water and extracted with 50 mL of CH_2Cl_2. The combined organic phase was washed with water, dried over anhydrous $MgSO_4$, filtered, and concentrated. Drying under vacuum gave compound 4 (4.50 g, 26.7 mmol, 96%) as a colorless oil. ^{1}H NMR (300 MHz, $CDCl_3$, δ): 7.10 (m, 1H), 6.90 (m, 1H), 6.77 (m, 1H), 2.82 (t, 2H), 1.67 (m, 2H), 1.34 (m, 6H), 0.89 (t, 3H).

2.2.5. Synthesis of 5-tributylstannyl-2-hexylthiophene (5)

Compound 4 (3 g, 17.8 mmol) was dissolved in 20 mL of anhydrous THF in a rounded-bottom flask under a Ar atmosphere. 11.1 mL of n-BuLi (1.6 M in hexane) was added dropwise at −78 °C. After the solution was stirred for 1 h, tributyltin chloride (5.8 g, 17.8 mmol) was added in one portion. Then the reaction was warm to room temperature and stirred for 15 h. Finally, the solution was purged into cold water. The organic phase was separated, and the aqueous layer was extracted with 50 mL of ether twice. The organic layers were collected and dried over anhydrous $MgSO_4$. After the solvent was removed, the crude product was purified by passing through Al_2O_3 column, using hexane as eluent. A colorless oil of 5-tributylstannyl-2-hexylthiophene was obtained (7.54 g, 93%). ^{1}H NMR (300 MHz, $CDCl_3$, δ):

6.98 (d, 1H), 6.88 (d, 1H), 2.85 (t, 2H), 1.70 (m, 2H), 1.56 (m, 6H), 1.34 (m, 12H), 1.08 (m, 6H), 0.92 (m, 12H).

2.2.6. Synthesis of 5-hexyl-2,2′-bithiophene (6)

Compound 6 was synthesized by the same procedure for synthesis of compound 4. Product was a light green liquid (yield 87%). ^{1}H NMR (300 MHz, $CDCl_3$, δ): 7.24–7.08 (m, 2H), 7.02–6.88 (m, 2H), 6.67–6.63 (d, 1H), 2.80–2.74 (t, 2H), 1.70–1.65 (m, 2H), 1.40–1.26 (m, 6H), 0.91–0.87 (t, 3H).

2.2.7. Synthesis of 5-hexyl-5′-trimethylstannyl-2,2′-bithiophene (7)

n-BuLi (2.5 M in hexanes, 4.58 ml, 11.4 mmol) was added dropwise over 15 min to a solution of compound 6 (2.58 g, 10.4 mmol) in anhydrous THF that was cooled at −78 ℃ under argon gas. The reaction mixture was stirred at −78 ℃ for 1 h and then trimethyltin chloride (1.0 M in THF) (12.5 ml, 12.5 mmol) was added in one portion as a solid. The mixture was warmed to room temperature and stirred for 12 h. Na_2CO_3 solution was added and then the aqueous phase was extracted with hexane. The organic extracts were dried over anhydrous $MgSO_4$. After filtration and evaporation of solvent, the product 7 was obtained as green oil (2.30 g, 49%). ^{1}H NMR (300 MHz, $CDCl_3$, δ): 7.18 (d, 1H), 7.05 (d, 1H), 6.96 (d, 1H), 6.63 (d, 1H) 2.76 (t, 2H) 1.66 (t, 2H) 1.34 (m, 6H), 0.88 (t, 3H), 0.38 (m, 9H)

2.2.8. Synthesis of eI-$(T)_2$ (8)

The compound 3 (50 mg, 0.060 mmol), the compound 5 (55 mg, 0.012 mmol) and tri(*o*-tolyl)phosphine (P(*o*-tyl)$_3$) (1.5 mg) in anhydrous toluene (4 mL) were charged in microwave reactor vial. The solution was degassed for 30 min and tris(dibenzylideneacetone)dipalladium(0) ($Pd_2(dba)_3$) (1.1 mg) was added. The mixture was heated at 120 ℃ for 4 h in microwave reactor. After reaction, mixture was cooled down to room temperature. Reaction solvent was removed and crude product was purified by silica chromatography with eluent (CH_2Cl_2:hexane = 2:1) to give compound 8 as a dark green solid (57 mg, 94%). ^{1}H NMR (300 MHz, $CDCl_3$, δ): 7.67 (d, 2H), 7.61 (s, 2H), 7.49 (d, 2H), 7.46 (d, 2H), 7.28 (d, 2H), 7.17 (d, 2H), 7.02 (s, 2H), 6.78 (d, 2H), 3.77 (d, 4H), 2.22 (m, 4H), 1.93 (m, 2H), 1.69 (m, 4H), 1.40–1.34 (m, 28H), 0.99–0.86 (m, 18H). ^{13}C NMR (125 MHz, $CDCl_3$, δ): 167.19, 146.46, 144,66, 142.66, 142.03, 138.55, 138.38, 135.26, 127.16, 125.46, 125.41, 123.53, 123.13, 121.26, 119.29, 119.05 105.67, 44.34, 38.09, 37.98, 31.84, 31.04, 30.56, 29.93, 29.11, 24.51, 23.32, 22.80, 14.33, 11.12, 10.97. MALDI–TOF MS (m/z): theory: 1009.54, found: 1009.77 $[M + H]^+$. Elemental anal. calcd. for ($C_{62}H_{76}N_2O_2S_4$): C, 73.70; H, 7.53; N, 2.77; O, 3.17; S, 12.68. Found: C, 73.72; H, 7.69; N, 2.70; S, 12.51%.

2.2.9. Synthesis of eI-$(2T)_2$ (9)

The compound 3 (44 mg, 0.072 mmol), the compound 7 (60 mg, 0.144 mmol) and tri(*o*-tolyl)phosphine (P(*o*-tyl)$_3$) (1.8 mg) in anhydrous toluene (5 mL) were charged in microwave reactor vial. The solution was degassed for

30 min and tris(dibenzylideneacetone)dipalladium(0) ($Pd_2(dba)_3$) (1.3 mg) was added. The mixture was heated at 120 ℃ for 4 h in microwave reactor. After reaction, mixture was cooled down to room temperature. Reaction solvent was removed and crude product was purified by silica chromatography with eluent (CH_2Cl_2:hexane = 2:3) to give compound 8 as a dark green solid (45 mg, 53%). ^{1}H NMR (300 MHz, $CDCl_3$, δ): 7.67 (d, 2H), 7.61 (s, 2H), 7.49 (d, 2H), 7.46 (d, 2H), 7.37 (d, 2H), 7.21 (d, 2H), 7.11 (d, 2H), 7.06 (d, 2H), 7.02 (s, 2H), 6.71 (d, 2H), 3.74 (m, 4H), 2.81 (m, 4H), 1.93 (m, 2H), 1.72 (m, 4H), 1.38–1.34 (m, 28H), 0.99–0.90 (m, 18H). ^{13}C NMR (125 MHz, $CDCl_3$, δ): 167.13, 145.98, 144,80, 143.46, 142.68, 138.75, 138.38, 134.55, 128.15, 127.49, 125.51, 125.09, 124.91 ,124.11, 124.08, 123.81, 123.45, 121.10, 119.34, 119.08, 105.61, 44.36, 38.11, 37.99, 31.80, 31.15, 30.44, 29.93, 29.09, 24.52, 23.34, 22.80, 14.37, 11.12, 10.96 MALDI–TOF MS (m/z): theory: 1173.79, found: 1173.43 $[M + H]^+$. Elemental anal. calcd. for ($C_{70}H_{80}N_2O_2S_6$): C, 71.56; H, 6.82; N, 2.39; O, 2.73; S, 16.36. Found: C, 71.63; H, 6.85; N, 2.40; S, 16.42%.

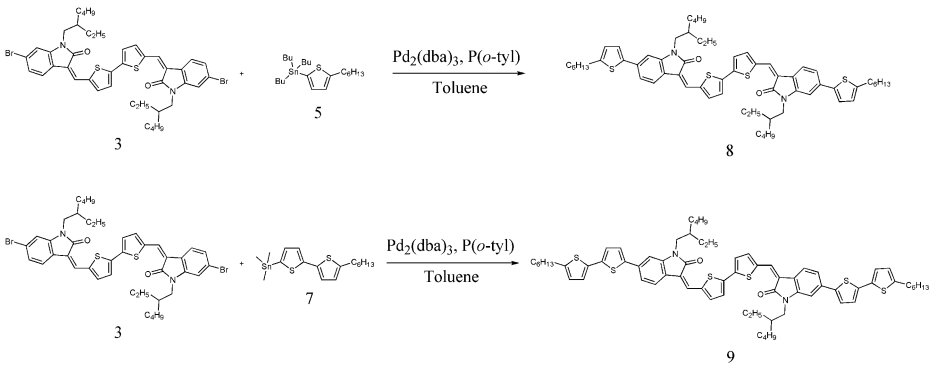

Scheme 2.3 The synthetic scheme of small-molecules

2.3. Synthesis of polymers

Extended isoindigo-based polymers, PeI-1T (15) and PeI-3T (16), were synthesized via Stille coupling between dibrominated eI-based monomers (12 and 14) and bisstannylated thiophene (10).

2.3.1. Synthesis of 2,5-bis-trimethylstannanyl-thiophene (10)

To a 100 ml two-neck round-bottomed flask under nitrogen atmosphere was added 2,5-dibromothiophene (2.0 g, 8.3 mmol) in dried THF (20 mL) at −78 ℃ under argon gas. 2.2 equiv. of n-butyllithium (7.3 ml, 18.2 mmol, 2.5 M in hexane) was added dropwisely to a solution. After that, the reaction mixture was stirred for 1 h. 2.2 equiv. of trimethyltin chloride (18.2 ml, 18.2 mmol, 1.0 M in THF) was added dropwisely. After stirring overnight at room temperature, reaction mixture was quenched with NH_4Cl (aq) and extracted with Et_2O. The organic layer was washed with water and brine then dried over $MgSO_4$. The crude compound was purified by recrystallization using ethanol to afford the compound 10 (2.30 g, 68%) as a needle-like white powder: ^1H NMR (300 MHz, $CDCl_3$, δ): 7.34 (s, 2H), 0.39 (s, 18H).

2.3.2. Synthesis of tributyl(4-octylthiophen-2-yl)stannane (11)

To a 100 ml two-neck round-bottomed flask under nitrogen atmosphere was added 3-octylthiophene (1.96 g, 10.0 mmol) in dried THF (20 mL) at −78 ℃ under argon gas. 1.0 equiv. of n-butyllithium (4 ml, 10.0 mmol, 2.5 M in hexane) was added dropwisely to a solution after which the reaction mixture was stirred for 15 min. After increasing to room temperature for 1 h, the mixture was then cooled to −78 ℃ again. 1.1 equiv. of tributyltin

chloride (3.55 g, 11.0 mmol) was added dropwisely and stirred for another 1 h. After stirring overnight at room temperature, reaction mixture was quenched with 2 M aqueous sodium hydrogen carbonate (10ml). After that, THF was removed and solution was extracted with dichloromethane. The organic layer was washed with water and brine then dried over $MgSO_4$. After removing solvent, the residue was purified on a column of neutral alumina with eluent hexane to afford the compound 11 (3.2 g, 66%) as a colorless oil. It was used in the next step without further purification.

2.3.3. Synthesis of 1-bromo-2-decyltetradecane (12)

2-Decyl-1-tetradecanol (20.0 g, 56.4 mmol) and triphenylphosphine (17.8 g, 67.8 mmol) were dissolved in dichloromethane (125 ml) and cooled in ice-water bath. To the mixture *N*-bromosuccinimide (NBS) (12.1 g, 67.8 mmol) was added slowly, then stirred at room temperature for 24 h. Removal of the solvent afforded the crude product which was further purified using column chromatography on silica gel using a hexane as eluent, giving the product as colorless oil. (21.5 g, 91.3%) ^{1}H NMR (300 MHz, $CDCl_3$,δ): 3.45 (d, 2H), 1.59 (m, 1H), 1.27 (m, 40H), 0.90 (m, 6H)

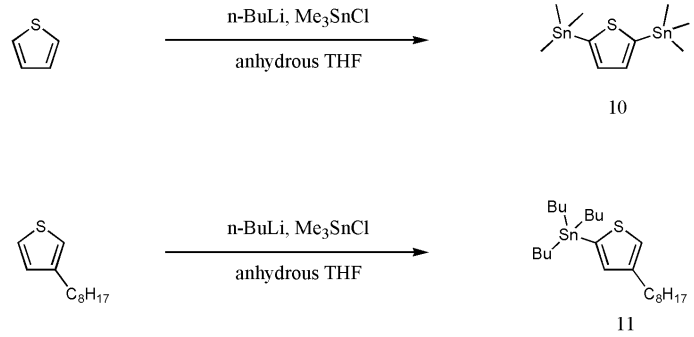

Scheme 2.4 The synthetic scheme of electron-rich units of polymers

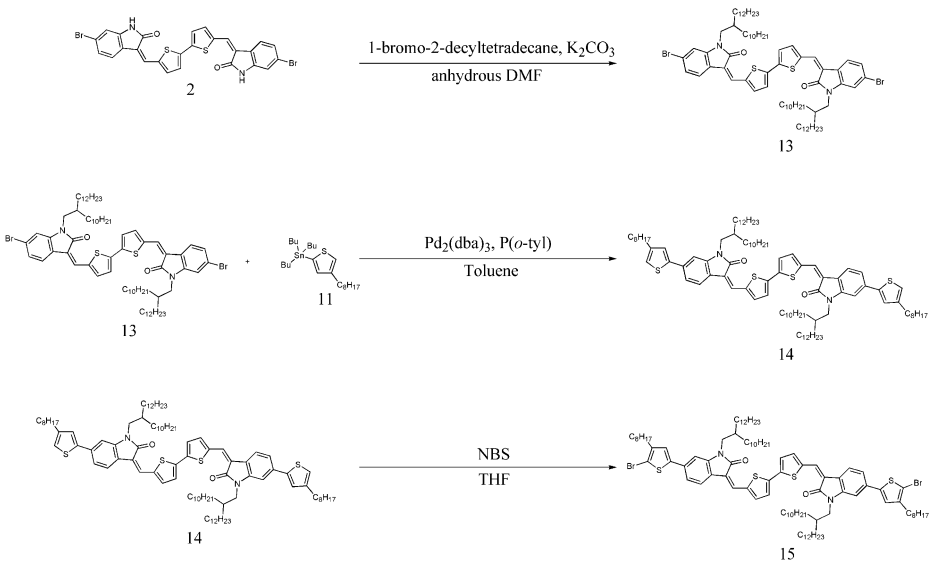

Scheme 2.5 The synthetic scheme of electron-deficient units of polymers

2.3.4. Synthesis of (3Z,3′Z)-3,3′-(2,2′-bithiophene-5,5′-diylbis-(methan-1-yl-1-ylidene))bis(6-bromo-1-(2-decyltetradecyl)indolin-2-one) (13)

Anhydrous potassium carbonate (2.26 g, 13.4 mmol) and compound 2 (2.00 g, 3.3 mmol) were dissolved in anhydrous DMF (40 mL) bubbled with argon for 20 minutes. The solution was heated at 120 ℃ for 1 h under argon. Compound 12 (4.10 g, 9.83 mmol) was added dropwise and the mixture was heated at 120 ℃ for 24 h. It was cooled to room temperature and was poured into water (300 mL). The mixture was extracted with dichloromethane. The combined organic layer was collected and was dried with $MgSO_4$. The solvent was removed under reduced pressure and the residue was purified by silica chromatography with eluent (CH_2Cl_2: hexane = 1:1) to give compound 13. (850 mg, 20%) ^{1}H NMR (300 MHz, $CDCl_3$, δ): 7.67 (d, 2H), 7.64 (s, 2H), 7.47 (d, 2H), 7.38 (d, 2H), 7.19 (d, 2H), 6.98 (s, 2H), 3.69 (d, 4H), 1.90 (m, 2H), 1.31–1.23 (m, 80H), 0.88–0.84 (m, 12H).

2.3.5. Synthesis of (3Z,3′Z)-3,3′-(2,2′-bithiophene-5,5′-diylbis-(methan-1-yl-1-ylidene))bis(1-(2-decyltetradecyl)-6-(4-octylthiophen-2-yl)-indolin-2-one) (14)

The compound 13 (240 mg, 0.187 mmol), the compound 11 (454 mg, 0.935 mmol) and tri(*o*-tolyl)phosphine (P(*o*-tyl)$_3$) (4.6 mg) in anhydrous THF (10 mL) were charged in a 100 ml two-neck round-bottomed flask. The solution was degassed for 30 min and tris(dibenzylideneacetone)dipalladium(0) ($Pd_2(dba)_3$) (3.4 mg) was added.

The mixture was heated at 80 ℃ overnight. After reaction, mixture was cooled down to room temperature. Reaction solvent was removed and crude product was purified by silica chromatography with eluent (CH_2Cl_2:hexane = 2:3) to give compound 14 as a dark purple solid (250 mg, 88%). ^{1}H NMR (300 MHz, $CDCl_3$, δ): 7.67 (d, 2H), 7.62 (s, 2H), 7.48 (d, 2H), 7.45 (d, 2H), 7.28 (d, 2H), 7.18 (s, 2H), 7.04 (s, 2H), 6.90 (s, 2H), 3.76 (d, 4H), 2.63 (m, 4H), 1.97 (m, 2H), 1.67 (m, 4H), 1.36 (m, 20H), 1.28–1.22 (m, 80H), 0.89–0.85 (m, 18H).

2.3.6. Synthesis of (3Z,3′Z)-3,3′-(2,2′-bithiophene-5,5′-diylbis-(methan-1-yl-1-ylidene))bis(1-(2-decyltetradecyl)-6-(5-bromo-4-octylthiophen-2-yl)-indolin-2-one) (15)

To a solution of compound 14 (180 mg, 0.12 mmol) in 30 ml anhydrous THF, NBS (47 mg, 0.24 mmol) was added separately in one of eight portions with an interval of 15 min. After 12 h reaction at room temperature, the reaction solution was evaporated by using rotary evaporator. The residue was purified by silica chromatography with eluent (CH_2Cl_2:hexane = 2:3) to give compound 15 as a dark purple solid. It was dried in a vacuum oven at 40 ℃ for 1 day to yield the pure product (122 mg, 61%). ^{1}H NMR (300 MHz, $CDCl_3$, δ): 7.67 (d, 2H), 7.63 (s, 2H), 7.50 (d, 2H), 7.46 (d, 2H), 7.20 (d, 2H), 7.02 (s, 2H), 6.94 (s, 2H), 3.76 (d, 4H), 2.58 (m, 4H), 1.93 (m, 2H), 1.63 (m, 4H), 1.35 (m, 20H), 1.26–1.22 (m, 80H), 0.89–0.86 (m, 18H).

2.3.7. Synthesis of PeI-1T (15)

The compound 13 (200 mg, 0.156 mmol), the compound 10 (64 mg, 0.156 mmol) and tri(*o*-tolyl)phosphine (P(*o*-tyl)$_3$) (4.5 mg) in anhydrous toluene (8 mL) were charged in microwave reaction vessel. The solution was degassed for 30 min and tris(dibenzylideneacetone)dipalladium(0) ($Pd_2(dba)_3$) (3.0 mg) was added. The mixture was heated at 150 ℃ for 5 h in microwave reactor. After the reaction was complete, the polymer was precipitated in cool methanol (250ml) and followed by sequent Soxhlet extraction of methanol, acetone, hexane, ethyl acetate to remove impurities until the extracts were colorless. Then, the polymer was extracted with chloroform. The chloroform fraction was reduced in volume and precipitated in methanol. Finally PeI-1T was dried in a vacuum oven at 40 ℃ for 1 day to yield the corresponding product (190 mg, 80%). Elemental anal. calcd. for $(C_{78}H_{110}N_2O_2S_3)$n: C 77.75, H 9.14, N 2.33, S 7.97%; found: C 76.46, H 9.31, N 2.20 S 7.51%. GPC: M_n=149kDa, PDI=1.84

2.3.8. Synthesis of PeI-3T (16)

The compound 15 (110 mg, 0.060 mmol), the compound 10 (25 mg, 0.060 mmol) and tri(*o*-tolyl)phosphine (P(*o*-tyl)$_3$) (3.0 mg) in anhydrous toluene (6 mL) were charged in microwave reaction vessel. The solution was degassed for 30 min and tris(dibenzylideneacetone)dipalladium(0) ($Pd_2(dba)_3$) (2.0 mg) was added. The mixture was heated at 150 ℃ for 5 h in microwave reactor. After the reaction was complete, the polymer was precipitated in cool methanol (250ml) and followed by sequent Soxhlet

extraction of methanol, acetone, hexane and ethyl acetate to remove impurities until the extracts were colorless. Then, the polymer was extracted with chloroform. The chloroform fraction was reduced in volume and precipitated in methanol. Finally PeI-3T was dried in a vacuum oven at 40 ℃ for 1 day to yield the corresponding product (72 mg, 76%). Elemental anal. calcd. for $(C_{102}H_{146}N_2O_2S_5)n$: C 76.86, H 9.17, N 1.76, S 10.05%; found: C 76.07, H 9.34, N 1.75 S 10.11%. GPC: M_n=108 kDa, PDI=1.97

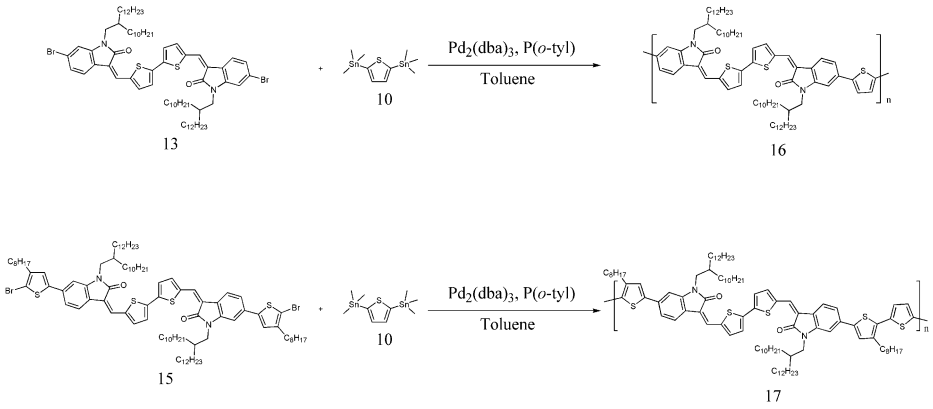

Scheme 2.6 The synthetic scheme of polymers

2.4. Characterization

The chemical structures of the monomers and small-molecules were identified by ^{1}H NMR (Avance DPX-300) and ^{13}C NMR (Avance DPX-500). Mass analysis and element analysis about synthesized materials were performed using MALDI TOF-TOF 5800 system and Flash2000 respectively. Molecular weight and its distribution were measured by gel permeation chromatography (GPC) (Waters) equipped with a Waters 2414 refractive index detector using $CHCl_3$ as an eluent, where the columns were calibrated against standard polystyrene samples. The optical absorption spectra were obtained by UV-Vis spectrophotometer (Lambda 25, Perkin Elmer). Cyclic voltammetry experiments were carried out on potentiostat/galvanostat (VMP 3 Biologic) in an electrolyte solution of 0.1 M tetrabutylammonium hexafluorophosphate (Bu_4NPF_6) in acetonitrile. A three-electrode setup was used with platinum wires (Bioanalytical System Inc.) both as working and counter electrode. Ag/Ag^+ was used as reference electrode calibrated with ferrocene/ferrocenyl couple (Fc/Fc^+). X-ray diffraction (XRD) patterns were obtained from an X-ray diffractometer (New D8 Advance, Bruker) using Cu-Kα radiation (λ= 1.5418 Å) at a scan rate of 2° min^{-1}. Thin film morphology was characterized by transmission electron microscopy (TEM) with a JEOL JEM1010 operating in 80 kV of acceleration voltage. For TEM measurement, the solar cell device was immersed in deionized water and then the active layer was floated onto the Cu grid. Density functional theory (DFT) calculation at the B3LYP/6-31G (d,p) level was performed using Gaussian 09 software.

2.5. Device fabrication and measurements

2.5.1. Materials

ITO-patterned glass was used as an anode in OPV device. The sheet resistance of the ITO was less than 10 Ω sq^{-1}. [6,6]-phenyl-C_{61}-butyric acid methyl ester ($PC_{61}BM$) (>99.5%) was obtained from Nano-C and used as received. PEDOT:PSS (Clevios P VP AI 4083) was purchased from H.C. Stark and passed through a 0.45 μm PVDF syringe filter before spin-coating. 1,8-Diiodooctane (DIO) was purchased from TCI chemicals.

2.5.2. Solar cell device fabrication

Photovoltaic devices were fabricated on ITO coated glass substrate with a layered structure of ITO/PEDOT:PSS/donor material:$PC_{61}BM$/Ca/Al. The ITO coated glass substrate was cleaned by stepwise sonication in deionized water, acetone and IPA for 15 min each. After complete drying, the ITO coated glass substrate was treated with UV-ozone for 15 min. PEDOT:PSS was spin-coated onto the ITO with 40 nm in thickness, and the substrate was annealed at 150 ℃ for 20 min. The solutions of eI-$(T)_2$ blended with $PC_{61}BM$ and PeI-1T blended with $PC_{61}BM$ were prepared at 2.0wt% concentration in anhydrous chlorinated solvent. And eI-(2T)2 and PeI-3T were prepared at 1.5wt% concentration. The solutions were stirred for 1 day at least. Then solution was spin-coated on the top of the PEDOT:PSS layer. 20nm calcium and 100 nm aluminum for cathode were thermally evaporated on the top of the active layer through a shadow mask under the pressure of

4×10^{-6}torr to fabricate devices with active area of ca. 4 mm^2.

2.5.3. Solar cell performance measurements

The photovoltaic performance was measured under nitrogen atmosphere inside the glove box. The current density–voltage (*J*–*V*) characteristic curves of the devices were obtained on a computer-controlled Keithley 4200 source measurement unit under AM 1.5G (100 mW cm^{-2}) simulated by an Oriel solar simulator (Oriel 91160A). The light intensity was calibrated using a NREL-certified photodiode prior to each measurement. The external quantum efficiency (EQE) was measured using Polaronix K3100 IPCE measurement system (McScience). The light intensity at each wavelength was calibrated with a standard single-crystal Si cell.

2.5.4. Device fabrication for hole mobility measurement by SCLC

Space charge limited current (SCLC) model by choosing high work function materials ITO and Au as electrodes was used Devices were fabricated on ITO coated glass substrate with a layered structure of ITO/PEDOT:PSS/polymer:$PC_{61}BM$/Au. The ITO coated glass substrate was cleaned by stepwise sonication in deionized water, acetone and IPA for 15 min each. After complete drying, the ITO coated glass substrate was treated with UV-ozone for 15 min. PEDOT:PSS was spin-coated onto the ITO with 40 nm in thickness, and the substrate was annealed at 150 ℃ for 20 min. A mixture of donor materials and $PC_{61}BM$ was dissolved in anhydrous chlorinated solvent and stirred for 1 day at least. Then solution was spin-coated on the top of the PEDOT:PSS layer. Then Au (80 nm) was thermally

deposited on the active layer. The active area of cell was ca. 4 mm^2

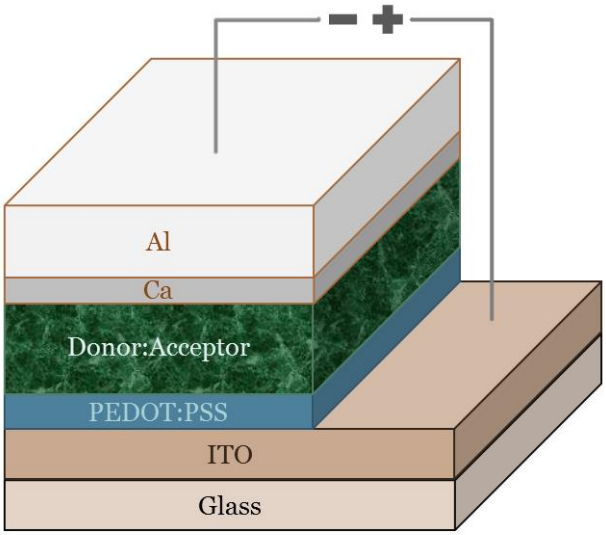

Fig 2.1 Schematic illustration of structure of OPV device

3. Result and Discussion

3.1. Synthesis and Charaterization

Extended isoindigo core (compound 2) was easily synthesized by Knoevenagel condensation reaction of 6-bromo-2-oxindole and 2,2′-bithiophene-5,5′-dicarbaldehyde. Due to strong π-π interaction, extended isoindigo has poor solubility in common organic solvent. To improve the solubility, the 2-ethylhexyl chains and 2-decyltetradecyl chains were attached to lactam nitrogen atom of extended isoingo of small-molecules (eI-$(T)_2$ and eI-$(2T)_2$) and polymers (PeI-1T, PeI-3T), respectively. In addition, to ensure solubility of PeI-3T, octyl group was attached to thiophene which is electron donating moiety of PeI-3T. A-D-A type small-molecules and D-A type alternating copolymers were synthesized from alkylated eI as electron-deficient unit and oligothiophene as electron-rich unit via microwave-assisted Stille coupling. The number-average molecular weight (M_n) and polydispersity index (PDI) of polymers are determined by Gel permeation chromatography (GPC) as shown in Table 3.1.

The chemical structure of 2,2′-bithiophene-5,5′-dicarbaldehyde (1), (3Z,3′Z)-3,3′-(2,2′-bithiophene-5,5′-diylbis-(methan-1-yl-1-ylidene))bis(6-bromo-1-(2-ethylhexyl)indolin-2-one) (3), 5-tributylstannyl-2-hexylthiophene (5), 5-hexyl-5′-trimethylstannyl-2,2′-bithiophene (7), eI-$(T)_2$ (8), eI-$(2T)_2$ (9), 2,5-bis-trimethylstannanyl-thiophene (10), tributyl(4-octylthiophen-2-yl)stannane (11), 1-bromo-2-decyltetradecane (12),

(3Z,3′Z)-3,3′-(2,2′-bithiophene-5,5′-diylbis-(methan-1-yl-1-ylidene))bis(6-bromo-1-(2-decyltetradecyl)indolin-2-one) (13), (3Z,3′Z)-3,3′-(2,2′-bithiophene-5,5′-diylbis-(methan-1-yl-1-ylidene))bis(1-(2-decyltetradecyl)-6-(4-octylthiophen-2-yl)-indolin-2-one) (14), (3Z,3′Z)-3,3′-(2,2′-bithiophene-5,5′-diylbis-(methan-1-yl-1-ylidene))bis(1-(2-decyltetradecyl)-6-(5-bromo-4-octylthiophen-2-yl)-indolin-2-one) (15) are identified by ^{1}H NMR, as shown in Figure 3.1-12, respectively.

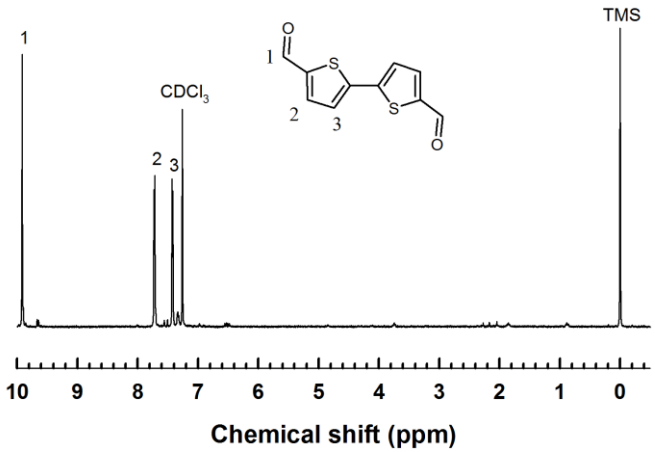

Fig 3.1 Chemical structure and ^{1}H NMR spectrum of compound 1

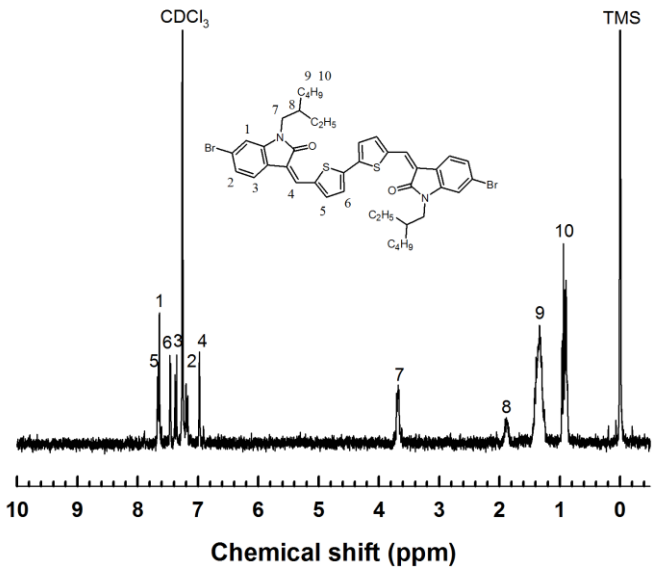

Fig 3.2 Chemical structure and 1H NMR spectrum of compound 3

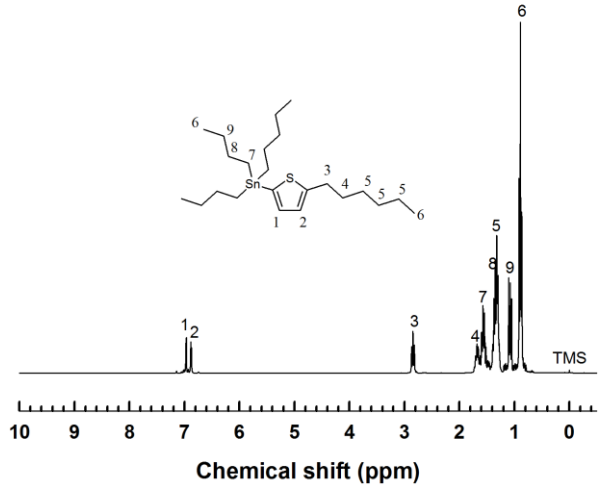

Fig 3.3 Chemical structure and ^{1}H NMR spectrum of compound 5

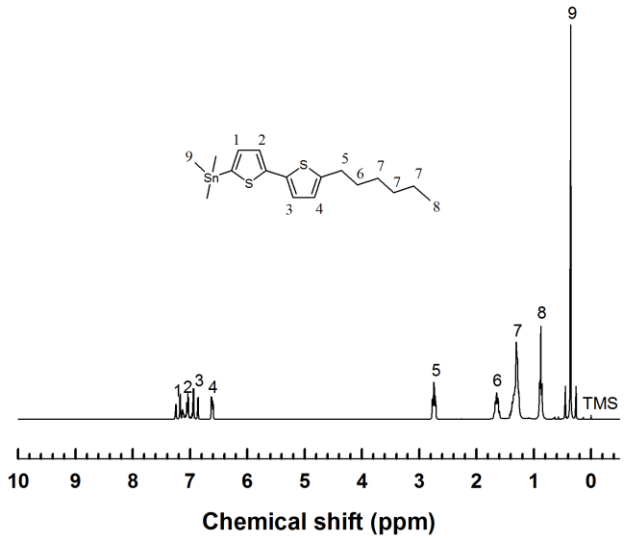

Fig 3.4 Chemical structure and ^{1}H NMR spectrum of compound 7

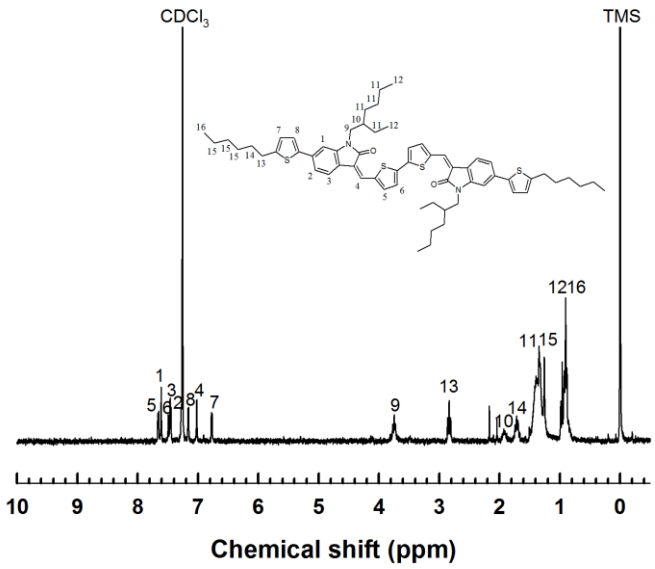

Fig 3.5 Chemical structure and ^{1}H NMR spectrum of compound 8

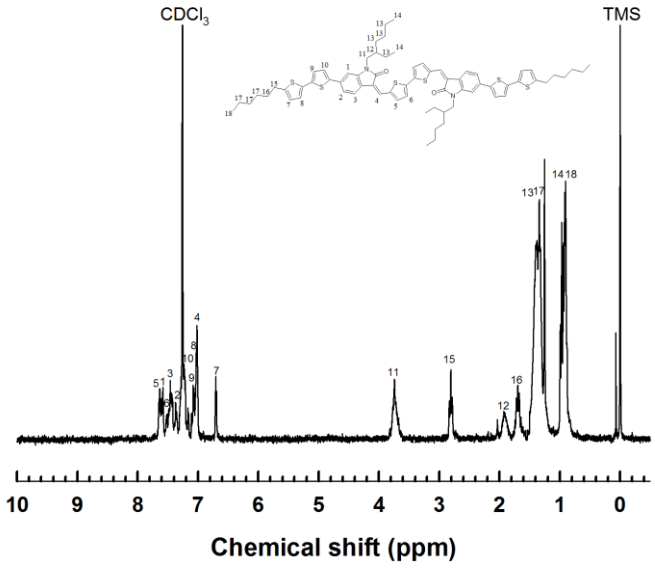

Fig 3.6 Chemical structure and ^{1}H NMR spectrum of compound 9

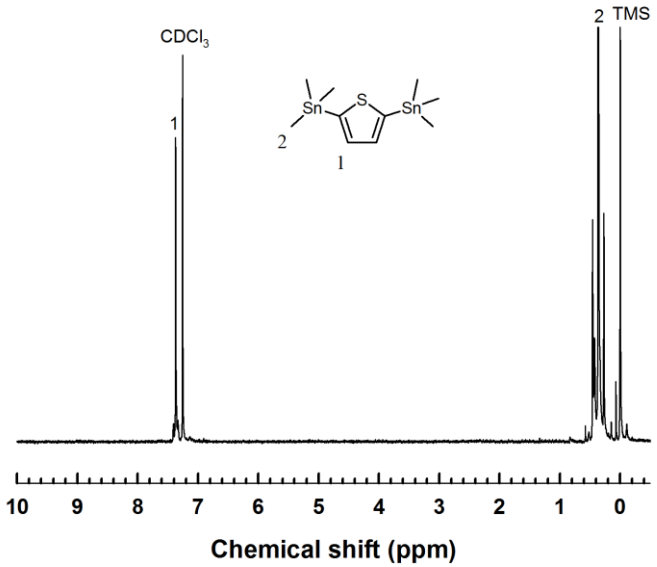

Fig 3.7 Chemical structure and ^{1}H NMR spectrum of compound 10

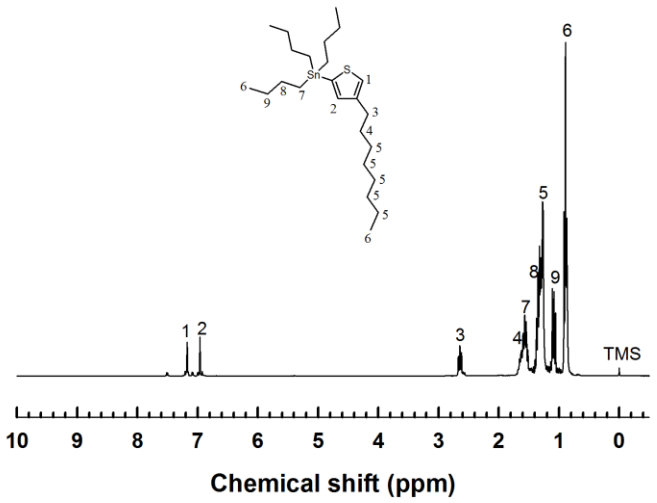

Fig 3.8 Chemical structure and ^{1}H NMR spectrum of compound 11

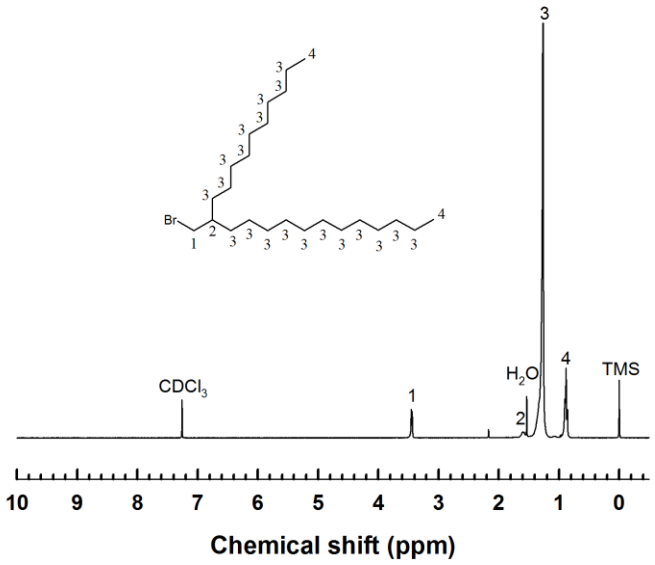

Fig 3.9 Chemical structure and ^{1}H NMR spectrum of compound 12

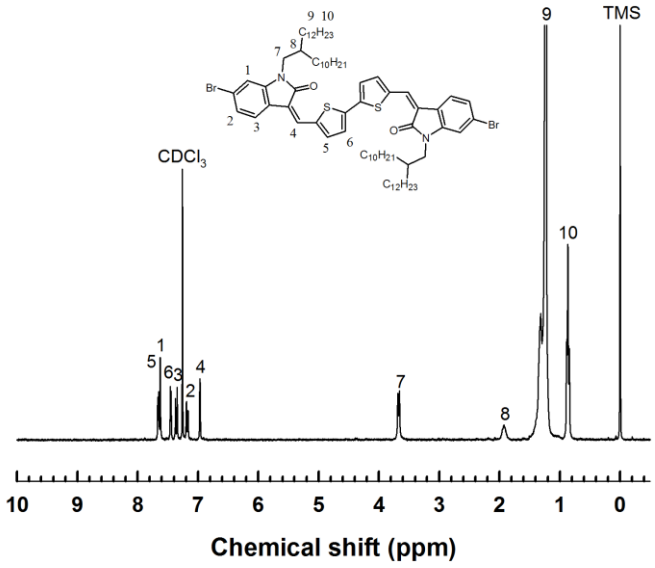

Fig 3.10 Chemical structure and ^{1}H NMR spectrum of compound 13

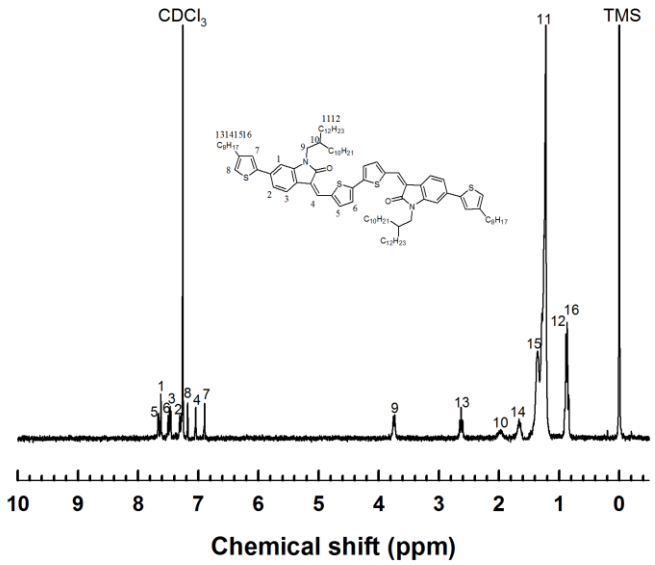

Fig 3.11 Chemical structure and ^{1}H NMR spectrum of compound 14

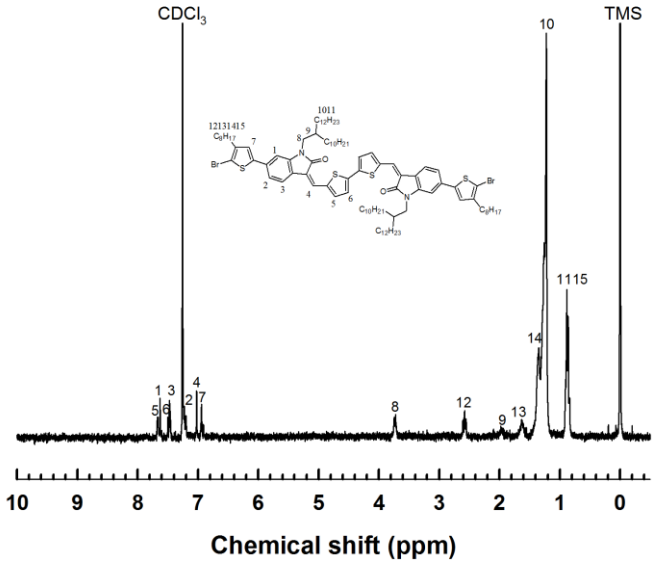

Fig 3.12 Chemical structure and ^{1}H NMR spectrum of compound 15

3.2. Optical properties

The optical characteristics of extended isoindigo based materials were investigated using UV-Vis absorption spectroscopy in dilute $CHCl_3$ solution (~10^{-5} M) and film. Summarized optical properties are represented in Table 3.1. The optical absorption spectra of eI-$(T)_2$, eI-$(2T)_2$, PeI-1T and PeI-3T in $CHCl_3$ solution (a, c) and in the solid state (b, d) are shown in Figure 3.13.

Small-molecules, eI-$(T)_2$ and eI-$(2T)_2$, showed absorption maximums (λ_{max}) at 548nm, 565nm with absorption coefficient 7×10^4 $M^{-1}cm^{-1}$ in solution. The absorption spectrum of eI-$(T)_2$ and eI-$(2T)_2$ in film was red-shifted compared to the solution spectrum and showed broad absorption in visible region. eI-$(T)_2$ and eI-$(2T)_2$ have shoulder peak at 620, 644nm, respectively. Polymers, PeI-1T and PeI-3T, showed absorption maximums at 606nm, 588nm with absorption coefficient 10×10^4 and 8×10^4 $Lg^{-1}cm^{-1}$ in solution, respectively. PeI-3T showed red-shifted (10nm) spectrum in the solid state.[36] PeI-1T and PeI-3T have shoulder peak at 658 nm. Not only extinction coefficient but also absorption in the visible region is important factor for donor materials of active layer of organic solar cells. Optical bandgaps of eI-$(T)_2$, eI-$(2T)_2$, PeI-1T and PeI-3T calculated from absorption onset (λ_{onset}) in film are 1.86, 1.74, 1.75 and 1.72 eV, respectively. Optical bandgap was decreased along with the conjugation length of the donor segment.

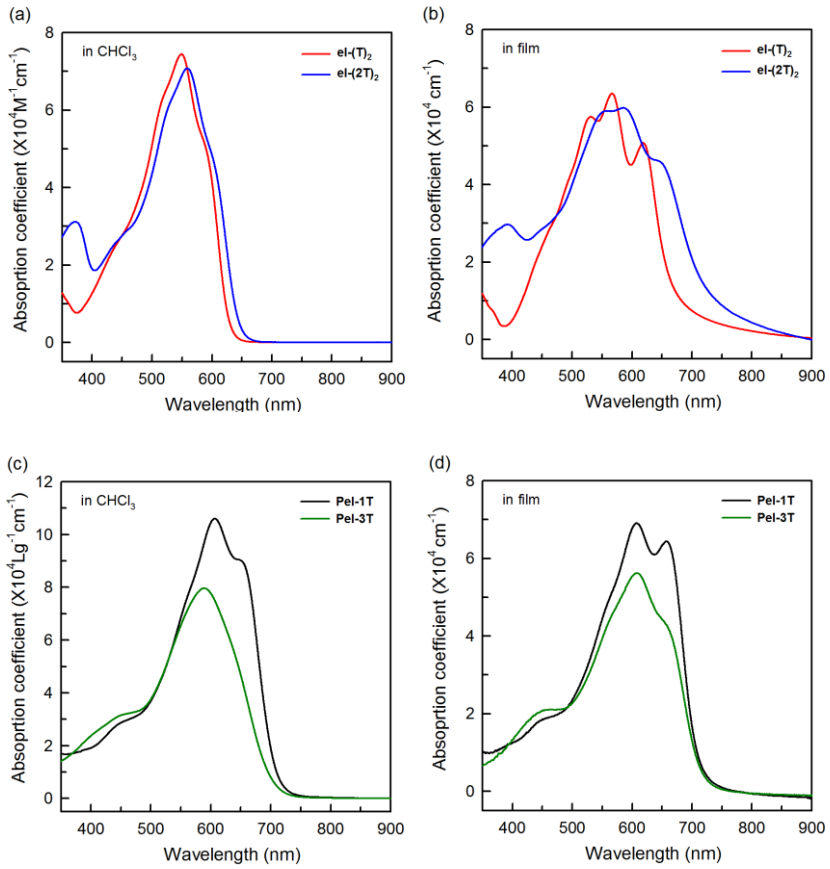

Fig 3.13 UV-Vis absorption spectrum of the small-molecules in $CHCl_3$ solution (a), small-molecules in film (b), polymers in $CHCl_3$ solution (c) and polymers in film (d).

3.3. Electrochemical properties

Cyclic voltammetry (CV) was performed to estimate the molecular energy levels (HOMO and LUMO) of eI-$(T)_2$, eI-$(2T)_2$, PeI-1T and PeI-3T. The energy level of the materials was calculated using the equation below:

$$HOMO = -[E_{ox} - E_{1/2}(ferrocene) + 4.8]\ eV,$$

$$LUMO = -[E_{red} - E_{1/2}(ferrocene) + 4.8]\ eV,$$

where E_{ox} is the onset oxidation potential of the material, E_{red} is the onset reduction potential of the material and $E_{1/2}$(ferrocene) is the onset oxidation of ferrocene vs. Ag/Ag^+. As shown in Figure 3.14, the HOMO energy levels of eI-$(T)_2$, eI-$(2T)_2$, PeI-1T and PeI-3T are –5.43, –5.25, –5.35 and 5.33 eV respectively. Since electron-donating strength of the donor groups were increased from eI-$(T)_2$ and PeI-1T to eI-$(2T)_2$ and PeI-3T, the HOMO energy levels were elevated. The open-circuit voltage (V_{oc}) of BHJ OPV is determined by the difference between HOMO energy level of donor and the LUMO energy level of acceptor.[37,38] The value of the LUMO energy level of material evaluated from CV is incorrect. Therefore the LUMO energy levels were calculated from the optical bandgap and HOMO energy level. The LUMO energy levels of eI-$(T)_2$, eI-$(2T)_2$, PeI-1T and PeI-3T are –3.57, –3.51, –3.60 and –3.61 eV, respectively. Extended isoindigo-based materials exhibited suitable LUMO energy levels for efficient charge transfer at the D/A interface. The offsets between the LUMO energy levels of donor materials and LUMO of PCBM (–4.0eV) are related to the driving force for the dissociation of exciton into free charge carries at the D/A interface, even

though the offset is not directly related to the driving force.[39] The LUMO energy offset of 0.3 eV is required to ensure efficient electron transfer from donor to PCBM.[40]

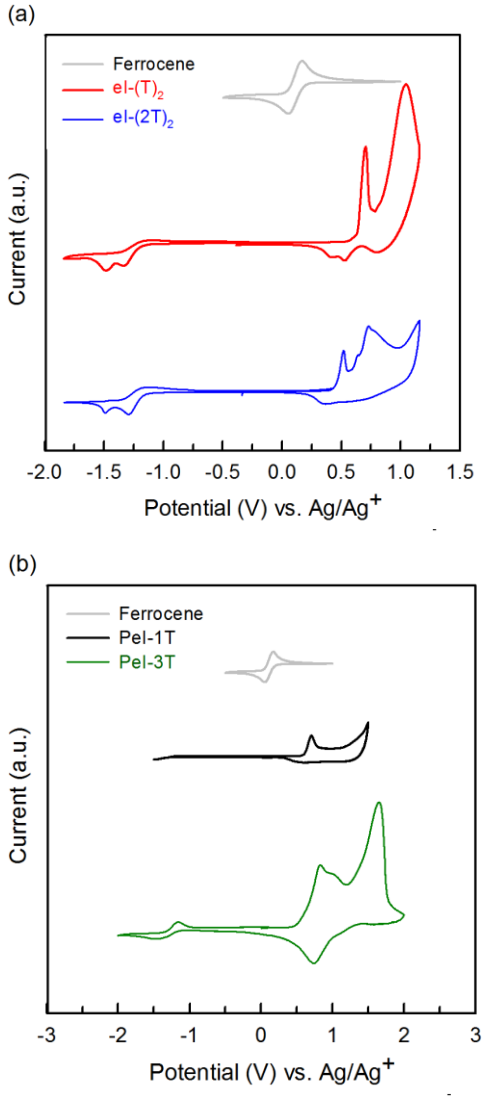

Fig 3.14 Cyclic voltammograms of small-molecules and polymers

Table 3.1 Optical and electrochemical properties of the polymers

Polymer	M_n (kg mol^{-1})	PDI	λ_{max} (nm)		E_g^{opt}[a]	HOMO	LUMO[b]	LUMO[c]
			solution	film	(eV)	(eV)	(eV)	(eV)
eI-$(T)_2$	-	-	548	565	1.86	–5.43	–3.57	–3.59
eI-$(2T)_2$	-	-	558	586	1.74	–5.25	–3.51	–3.25
PeI-1T	149	1.84	606	607	1.75	–5.35	–3.60	–3.47
PeI-3T	108	1.97	588	607	1.72	–5.33	–3.61	–3.61

[a] is optical bandgap in film.

[b] is calculated from the optical bandgap and the HOMO energy level. LUMO = HOMO + E_g^{opt}.

[c] is measured by cyclic voltammetry.

3.4. Structural properties

X-ray diffraction (XRD) analysis was performed to investigate the crystalline structure of pristine eI-$(T)_2$ and eI-$(2T)_2$, pristine PeI-1T and PeI-3T, blend eI-$(T)_2$ and eI-$(2T)_2$ with $PC_{61}BM$, blend PeI-1T and PeI-3T with $PC_{61}BM$. Figure 3.15 shows the XRD patterns of films which were thermally annealed at 120 ℃ for 10 min.

Extended isoindigo-based small-molecules exhibited strong diffraction peaks (100) at 2θ =5.24° for eI-$(T)_2$ and 2θ =5.37° for eI-$(2T)_2$, which correspond to the interchain distance separated by alkyl side chain (ethlyhexyl) of 16.84, and 16.43 Å, respectively. The *d*-spacing value was derived by using Bragg's law of $2d\sin\theta = \lambda$, herein λ=0.154 nm. Also low intensity of the second-order diffraction peaks (200) and the third-order diffraction peaks (300) for eI-$(T)_2$ and eI-(2T) was observed. The film of pristine eI-$(T)_2$ showed relatively lower crystallinity than eI-$(2T)_2$ while the film of blend eI-$(T)_2$ with $PC_{61}BM$ showed higher crystallinity than eI-$(2T)_2$. In the case of polymers, pristine films of PeI-1T and PeI-3T showed broad diffraction peak (010) at near 25° , which corresponds to the π-π stacking between polymer backbones. After blending with $PC_{61}BM$, (010) peak of polymers disappeared. The perfectly planar structure of extended isoindigo can be considered to have a positive influence on the molecular packing and crystallinity of extended isoindigo-based materials.

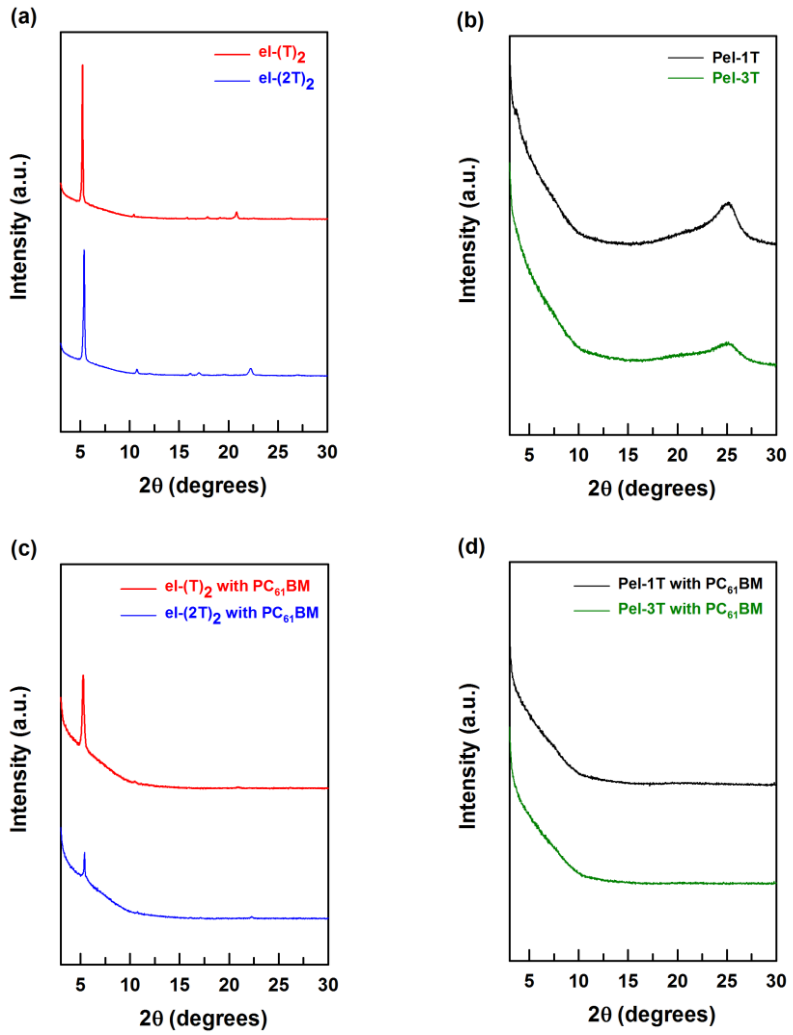

Fig 3.15 X-ray diffraction patterns of (a) pristine eI-$(T)_2$ and eI-$(2T)_2$, (b) pristine PeI-1T and PeI-3T, (c) blend eI-$(T)_2$ and eI-$(2T)_2$ with $PC_{61}BM$, (d) blend PeI-1T and PeI-3T with $PC_{61}BM$.

3.5. Photovoltaic properties

Photovoltaic properties of extended isoindigo-based materials was investigated using device with configuration of ITO/PEDOT:PSS/donor material:$PC_{61}BM$/Ca/Al (Figure. 2.1). The *J*–*V* characteristics of organic solar cells prepared from donor material:$PC_{61}BM$ using various solvents, chloroform (CF), chlorobenzene(CB) and 1,2-dichlorobenzene (*o*-DCB), are represented in Figure. 3.16. Photovoltaic parameters and optimized processing conditions of device fabrication are summarized in Table 3.2. The optimum weight ratios of the donor material:$PC_{61}BM$ were 2:1 for eI-$(T)_2$, 1.5:1 for eI-$(2T)_2$ and 1: 1 for polymers, respectively. The V_{OC}s of eI-$(T)_2$-based device and PeI-1T-based device are 0.71 V and 0.76 V, respectively, which are higher value than 0.69 V of eI-$(2T)_2$-based device and PeI-3T-based device. This result is in accordance with the deeper HOMO energy level of eI-$(T)_2$ and PeI-1T than eI-$(2T)_2$ and PeI-3T. The pre-annealed devices of eI-$(T)_2$:$PC_{61}BM$ blend(1:1) exhibit higher V_{OC} of 0.77 V but exhibit a less efficient photovoltaic performance of 1.53 % due to lower J_{SC} of 5.81 mA cm^{-2} than pre-annealed devices of eI-$(T)_2$:$PC_{61}BM$ blend(2:1). The BHJ solar cells fabricated from eI-$(T)_2$ and PeI-1T performed better than devices fabricated from eI-$(2T)_2$, and PeI-3T at the optimized processing conditions, respectively. The OPV device of PeI-1T with $PC_{61}BM$ exhibited a PCE of 4.06% with J_{SC} of 11.86 mA cm^{-2} and FF of 45%. The stronger extinction coefficient and thicker film of PeI-1T than PeI-3T can be the contributing factors to high J_{SC} of PeI-1T. The external quantum efficiency

(EQE) spectra of optimized devices under monochromatic light are shown in Figure 3.17. The EQE and absorption spectra exhibit similar tendency.

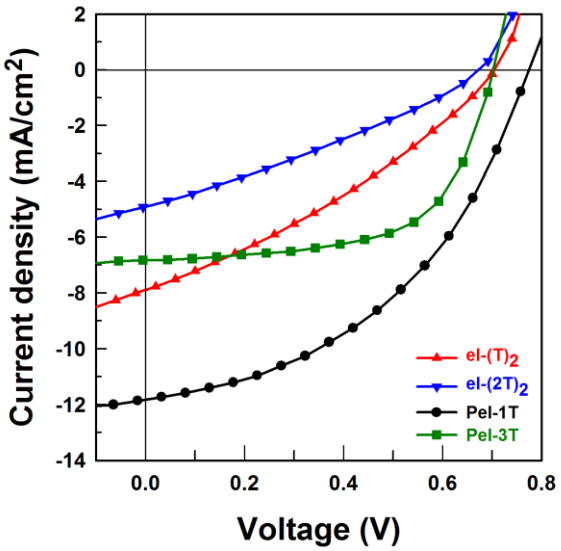

Fig 3.16 *J*–*V* curves measured under AM 1.5 G (100 mW cm^{-2}) of organic photovoltaic(OPV) devices based on eI-(T)$_2$, eI-(2T)$_2$, PeI-1T and PeI-3T

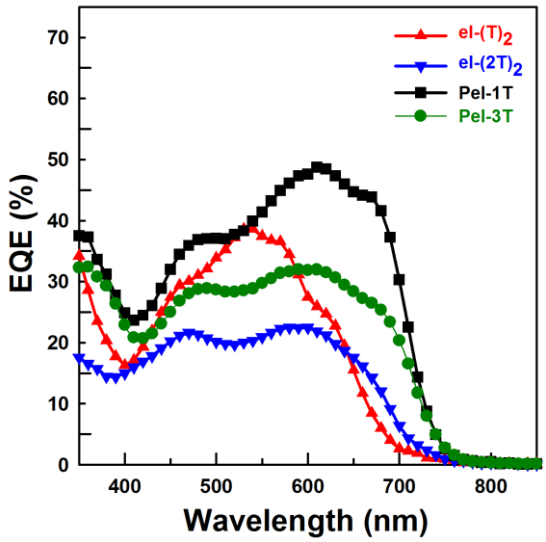

Fig 3.17 External quantum efficiency (EQE) curves of OPV devices with eI-$(T)_2$, eI-$(2T)_2$, PeI-1T and PeI-3T

Table 3.2 Summary of photovoltaic properties of eI-$(T)_2$, eI-$(2T)_2$, PeI-1T and PeI-3T blended with $PC_{61}BM$

Donor material	Solvent	Blend ratio (w/w)	V_{OC} (V)	J_{SC} (mA cm^{-2})	FF (%)	PCE[a] (%)	Hole mobility[b] ($cm^2V^{-1}s^{-1}$)
eI-$(T)_2$[c]	CB	2:1	0.71	7.90	32	1.80 (1.19)	3.69×10^{-4}
eI-$(2T)_2$	CB	1.5:1	0.69	4.93	29	0.99 (0.89)	2.20×10^{-4}
PeI-1T	*o*-DCB+DIO 2vol%	1:1	0.76	11.86	45	4.06 (3.85)	1.16×10^{-4}
PeI-3T	CF+DIO 3vol%	1:1	0.69	6.82	63	2.96 (2.81)	6.00×10^{-6}

[a] The PCE in parentheses are the average PCE from 4 devices.

[b] is measured by space-charge limited current method.

[C] Annealed at 100 °C for 20 min.

3.6. Charge transport characteristics

The carrier mobility is an important factor to determine the photovoltaic performance.[41,42] It is known that carrier mobility is influenced by various factors, such as polymer molecular weight (MW)[43], backbone planarity and ordering, vertical phase graduation.[44] Space charge limited current (SCLC) measurement was performed to investigate the hole mobility perpendicular to the substrate plane. The configuration of hole-only device was ITO/PEDOT:PSS/polymer:$PC_{61}BM$/Au. The hole mobility was obtained from the SCLC *J*–*V* curve and was calculated by the trap-free SCLC model at low reverse applied voltage in the dark. The SCLC behavior is analyzed using the Mott-Gurney law,[45,46]

$$J = (9/8)\varepsilon_0\varepsilon_r\mu_h(V^2/L^3)$$

where ε_0 is vacuum permittivity, ε_r is dielectric constant of the donor material (assumed 3), μ_h is drift mobility of charge carrier, $V = V_a - V_{bi}$ (V_a: applied bias, V_{bi}: built-in potential, herein, 0.2 V), and L is the thickness of the film. The hole mobilities of the eI-$(T)_2$, eI-$(2T)_2$, PeI-1T and PeI-3T calculated from *J*–*V* curve (Figure 3.14 (a)) are 3.69×10^{-4}, 2.20×10^{-4}, 1.16×10^{-4} and 6.00×10^{-6} $cm^2V^{-1}s^{-1}$, respectively. The higher hole mobility of the eI-$(T)_2$ is attributed to higher crystallinity of eI-$(T)_2$ than eI-$(2T)_2$ (as shown in Figure. 3.15 (c)). The high crystallinity of extended isoindigo-based materials contributes to the high mobility of the photovoltaic devices to some extent.

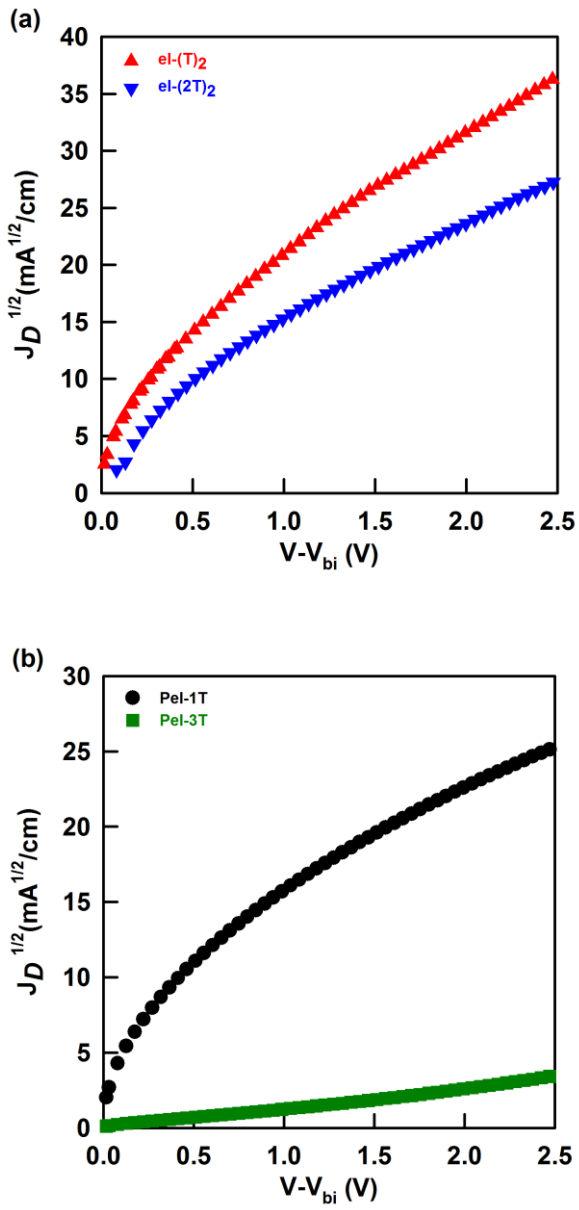

Fig 3.18 Dark current density–voltage curves from SCLC devices of polymer:$PC_{61}BM$ blend film

3.7. Morphology investigation

The morphology of thin film by solution processing has a tremendous impact on the photovoltaic properties. It is clear that controlling processing condition for optimized morphology needs to be conducted with meticulous care.[47] Optimal active layer morphology of fabricated device was controlled through the solvent selection, thermal annealing and incorporating additive.[48] To investigate the morphology of the blend film, transmission electron microscopy (TEM) was used. Figure 3.19 shows TEM images of film morphology of devices with the individual optimized conditions (see Table 3.2). The bright phase can be attributed to the donor material-rich region, while the dark phase can be attributed to the $PC_{61}BM$-rich region due to its high electron scattering density.[49] The eI-$(2T)_2$ film blended with $PC_{61}BM$ cast from CB exhibited a coarse morphology, as shown in Figure 3.19 (b), indicating the formation of large, segregated domains and poor network. To improve the morphology of film and PCE, heat treatment with various annealing time and temperature was performed on the eI-$(2T)_2$-based device and 1,8-diiodooctane (DIO) was added into the solution. However, poor power conversion efficiency was obtained. The polymer aggregates in blends trap excitons and hinder their dissociation because excitons generated in aggregated regions are difficult to diffuse to the D/A interface for charge separation. The reduced dissociation of excitons contributes to the BHJ device photocurrent.[52] On the other hand, pre-annealed eI-$(T)_2$:$PC_{61}BM$ blend film shows better morphology with better connected pathway. Interconnected network of eI-$(T)_2$:$PC_{61}BM$ blend film is attributed to higher

J_{sc} than eI-$(2T)_2$ because of efficient charge transport. In the case of polymers, PeI-1T:$PC_{61}BM$ blend film shows microphase separation, indicative of good miscibility between PeI-1T and $PC_{61}BM$ (Figure 3.16 (c)). This optimized morphology of PeI-1T-based device were realized by employing a small amount (2 vol.%) of DIO as additive. DIO additive could make PCBM more dispersive in the active layer.[50] The efficiency (4.06%) of PeI-1T-based device is ascribed to a fine-tuning of the blend morphology to some extent in terms of the formation of bi-continuous interpenetrating network, which prevents geminate and bimolecular recombination and promotes exciton dissociation and charge carrier transport.[51,52]

The film of PeI-3T–based device also exhibits nanomorphology. However, PeI-1T exhibited higher J_{SC} than PeI-3T due to thicker film and higher extinction coefficient. The photon absorption is directly related to the generation of exciton. Accordingly, PeI-3T-based organic solar cell exhibited lower PCE, even though showed higher FF, as compared to PeI-1T.

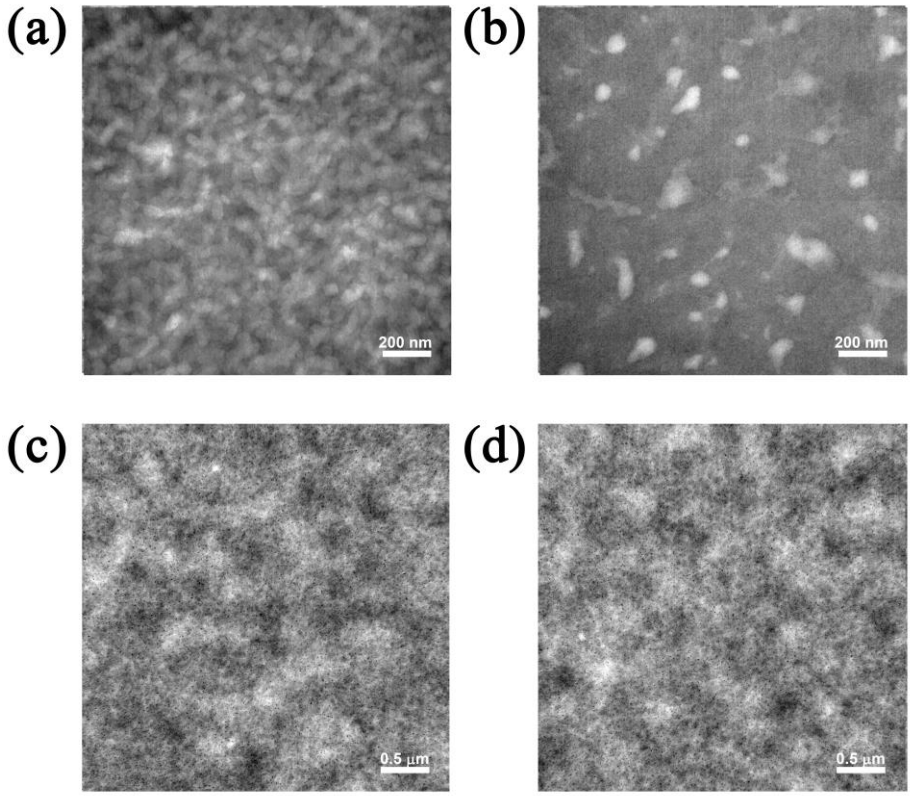

Fig 3.19 TEM images of eI-$(T)_2$:$PC_{61}BM$ (a), eI-$(2T)_2$:$PC_{61}BM$ (b), PeI-1T:$PC_{61}BM$ (c) and PeI-3T:$PC_{61}BM$ (d) at the optimized processing conditions

4. Conclusions

In this study, extended isoindigo-based small molecules and polymers for donor materials of organic photovoltaic devices were synthesized to investigate the photovoltaic properties based on optical, electrochemical, structural analysis. Extended isoindigo unit is synthesized from two oxindoles and 2,2′-bithiophene-5,5-dicarbaldehyde by a simple Knoevenagel condensation reaction and exhibits a weaker electron-accepting unit than isoindigo due to incorporating electron-donating unit of 2,2′-bithiophene. Extended isoindigo-based materials have the suitable LUMO energy level of −3.6 eV and the band gap of −1.75eV approximately. Furthermore, extended isoindigo-based materials show good π−π stacking behavior, which is attributed to the perfectly planar structure of extended isoindigo. Extended isoindigo-based small-molecule, eI-$(T)_2$, and polymer, PeI-1T, exhibit best PCE of 1.80% and 4.06% respectively owing to high photocurrent. These results demonstrate that extended isoindigo can be a promising building block for efficient organic solar cells.

Bibliography

(1) Brabec, C. J, Sariciftci, N. S, Hummelen, J. C, *Adv. Funct. Mater*. **2001**, 11, 15.

(2) G. Dennler, M. C. Scharber and C. J. Brabec, Adv. Mater. **2009**, 21, 1323–1338.

(3) Alan J. Heeger. *Adv. Mater.* **2014**, 26, 10–28.

(4) G. Yu, J. Gao, J. C. Hummelen, F. Wudl, A. J. Heeger, *Science* **1995**, 270, 1789.

(5) Gang. Li, Rui. Z, Yang.Y, *Nature Photon*. **2012**, 6, 153.

(6) I. Etxebarria, J. Ajuria and R. Pacios, *Org. Electron*., **2015**, 19, 34–60.

(7) Z. C. He, C. M. Zhong, S. J. Su, M. Xu, H. B. Wu and Y. Cao, *Nat. Photonics*, **2012**, 6, 591.

(8) C.-C. Chen, W.-H. Chang, K. Yoshimura, K. Ohya, J. You, J. Gao, Z. Hong and Y. Yang, *Adv. Mater.*, **2014**, 26, 5670.

(9) A. R. B. M. Yusoff, D. Kim, H. P. Kim, F. K. Shneider, W. J. Da Silva and J. Jang, *Energy Environ. Sci.*, **2015**, 8, 303–316.

(10) Xu. T, Yu. L, *Mater. Today* **2014**, 17, 11.

(11) Shaw, P. E, Ruseckas. A, Samuel. I. D, *Advanced Materials*, **2008**, 20, 3516-3520.

(12) W. L. Ma, C. Y. Y ang, X. Gong, K. Lee, A. J. Heeger, *Adv. Funct.*

Mater. **2005**, 15, 1617.

(13) C. J. Brabec, C. Winder, N. S. Sariciftci, J. C. Hummelen, A. Dhanabalan, P. A. van Hal, and R. A. J. Janssen, *Adv. Funct. Mater*. **2002**, 12, 709.

(14) Mihailetchi, V. D., Xie, H. X., de Boer, B., Koster, L. J. A., Blom,P. W, *Adv. Funct. Mater*. **2006**, 16, 699-708.

(15) Li, Y. F. Acc. Chem. Res. 2012, 45, 723−733

(16) C. Gao, L. Wang, X. Li, H. Wang. *Polym. Chem.*, **2014**, 5, 5200

(17) P. L. T. Boudreault, A. Najari and M. Leclerc, *Chem. Mater.*,**2011**, 23, 456–469.

(18) J. Mei, K. R. Graham, R. Stalder, J. R. Reynolds, *Org. Lett*. **2010**, 12, 660.

(19) G. Zhang, Y. Fu, Z. Xie, Q. Zhang, *Macromolecules* **2011**, 44, 1414.

(20) B. Liu, Y. Zou, B. Peng, B. Zhao, K. Huang, Y. He, C. Pan, *Polym. Chem.* 2011, 2, 1156.

(21) Ma, Z, Wang, E, Vandewal, K, Andersson, M. R, Zhang, F. *Appl. Phys. Lett.*, **2011**, 99, 143302.

(22) R. Stalder, J. Mei, K. R. Graham, L. A. Estrada, J. R. Reynolds, *Chem. Mater*., **2014**, 26, 664.

(23) E. G. Wang, W. Mammo, M. R. Andersson, *Adv. Mater*., **2014**, 26, 1801.

(24) Y. Deng, W. Li, L. Liu, H. Tian, Z. Xie, Y. Geng, F. Wang, *Energy Environ. Sci*., **2015**, 8, 585.

(25) Jung, E. H.; Jo, W. H. *Energy Environ. Sci*.. **2014**, 7, 650.

(26) Z. Ma, E. Wang, M. E. Jarvid, P. Henriksson, O. Inganaes, F. Zhang, M. R. Andersson, *J. Mater. Chem*. **2012**, 22, 2306.

(27) T. Wu, C. Yu, Y. Guo, H. Liu, G. Yu, Y. Fang and Y. Liu, *J. Phys.Chem. C*, **2012**, 116, 22655.

(28) P. K. Nayak, G. Garcia-Belmonte, A. Kahn, J. Bisquert and D. Cahen, *Energy Environ. Sci*., **2012**, 5, 6022–6039.

(29) Z. Ma, W. Sun, S. Himmelberger, K. Vandewal, Z. Tang, J. Bergqvist, A. Salleo, J. W. Andreasen, O. Inganas, M. R. Andersson, C. Muller, F. Zhang and E. Wang, *Energy Environ.Sci*., **2014**, 7, 361.

(30) C.-C. Ho, C.-A. Chen, C.-Y. Chang, S. B. Darling, W.-F. Su. *J. Mater. Chem.*, **2014**, 2, 8026–8032.

(31) Lei, T, Wang, J.-Y, Pei, J. *Acc. Chem. Res*. **2014**, 47, 1117.

(32) Lei, T, Dou, J.-H, Cao, X.-Y, Wang, J.-Y, Pei, J. *Adv. Mater*. **2013**, 25, 6589−6593.

(33) Li, S, Yuan, Z, Yuan, J, Deng, P, Zhang, Q, Sun, B, *J Mater. Chem. A*, **2014**, 2, 5427.

(34) Guo, X, Zhou, N, Lou, S. J, Hennek, J. W, Ortiz, R. P, Butler, M. R, Boudreault, P.-L. T, Strzalka, J, Morin, P.-O, Leclerc, M, Navarrete, J. T. L, Ratner, M. A, Chen, L. X, Chang, R. P. H, Facchetti, A, Marks,

T. J. *J. Am. Chem. Soc*., **2012**, 134, 18427.

(36) Ioan Botiz, Natalie Stingelin, *Materials*, **2014**, 7, 2273-2300.

(37) M. C. Scharber, D. Wuhlbacher, M. Koppe, P. Denk, C. Waldauf, A. J. Heeger, C. J. Brabec, *Adv. Mater*., **2006** , 18 , 789.

(38) C. J. Brabec, A. Cravino, D. Meissner, N. S. Sariciftci, T. Fromherz, M. T. Rispens, L. Sanchez, J. C. Hummelen, *Adv. Funct. Mater*., **2001** , 11 , 374.

(39) E. R. Bittner, J. G. S. Ramon, S. Karabunarliev, *J. Chem.Phys*., **2005**, 122, 214719.

(40) S. R. Cowan, A. Roy, A. J. Heeger, *Phys. Rev. B* **2010**, 82, 245207.

(41) J.-T. Shieh, C.-H. Liu, H.-F. Meng, S.-R. Tseng, Y.-C. Chao, and S.-F. Horng, *J. Appl. Phys*. **2010**, 107, 084503.

(42) L. M. Andersson, C. Müller, B. H. Badada, F. Zhang, U. Würfel and O. Inganäs, *J. Appl. Phys*., **2011**, 110, 024509.

(43) Ballantyne, A. M, Chen, L, Dane, J, Hammant, T, Braun, F. M, Heeney, M, Duffy, W, McCulloch, I, Bradley, D. D. C, Nelson, J. *Adv. Funct. Mater*., **2008**, 18, 2373.

(44) Guo, X, Zhou, N, Lou, S. J, Smith, J, Tice, D. B. Hennek, J. W, Ortiz, R. P, Navarrete, J. T. L, Li, S, Strzalka, J, Chen, L. X, Chang, R. P. H, Facchetti, A, Marks, T. J. *Nat. Photonics* **2013**, 7, 825−833.

(45) Shrotriya, V.; Wu, E. H. E.; Li, G.; Yao, Y.; Yang, Y. *Appl. Phys.*

Lett., **2006**, 88, 064104.

(46) Kymakis, E.; Servati, P.; Tzanetakis, P.; Koudoumas, E.; Kornilios, N.; Rompogiannakis, I.; Franghiadakis, Y.; Amaraunga, G. A. J. *Nanotechnology*, **2007**, 18, 435702.

(47) L.-M. Chen, Z. Hong, G. Li, Y. Yang, *Adv. Mater*. **2009**, 21, 1434.

(48) Liao, H.-C, Ho, C.-C, Chang, C.-Y, Jao, M.-H, Darling, S. B, Su, W.-F. *Mater. Today,* **2013**, 16, 326.

(49) Yang, X.; Loos, J.; Veenstra, S. C.; Verhees, W. J. H.; Wienk, M. M.; Kroon, J. M.; Michels, M. A. J.; Janssen, R. A. J. *Nano Lett*, **2005**, 5, 579.

(50) Lou, S. J, Szarko, J. M, Xu, T, Yu, L. P, Marks, T. J, Chen, L. X. *J. Am. Chem. Soc.* **2011**, 133, 20661−20663.

(51) A. Zusan, B. Gieseking, M. Zerson, V. Dyakonov, R. Magerle and C. Deibel, *Sci. Rep*., **2015**, 5, 8286

(52) Dyer-Smith, C, Howard, I. A, Cabanetos, C, Labban, A. E, Beaujuge, P. M, Laquai, F. *Adv. Energy Mater*. **2015**, 5, 1401778

초 록

본 연구에서는 유기태양전지 광활성층을 이루는 전자 주개 물질의 전자 받개 단위로 extended isoindigo를 활용하여 새로운 단분자와 고분자를 합성하였고 extended isoindigo기반의 전도성 물질에 대한 구조적, 전기화학적, 광전기적 특성을 관찰하였다. Extended isoindigo는 2,2′-bithiophene-5,5′-dicarbaldehyde와 두 개의 oxindole을 Knoevenagel 축합반응으로 결합시킨 전자 받개 단위이다. Extended isoindigo는 isoindigo의 전자 받개 능력을 감소시켜 isoindigo보다 LUMO 레벨이 상향되었다. Stille coupling을 통해 합성한 extended isoindigo기반의 전도성 단분자와 고분자는 –3.6 eV 내외의 적절한 LUMO 레벨과 1.75 eV 내외의 bandgap을 보여주었다. 또한 extended isoindigo 단위체는 DFT 계산을 통해 완벽한 평면구조를 갖고 있으며, 이를 기반으로 합성한 고분자들은 XRD 분석을 통해 좋은 π-π stacking을 나타내는 것을 확인하였다. Extended isoindigo기반의 물질들과 $PC_{61}BM$으로 제작한 벌크 이종접합 유기태양전지는 단분자인 eI-$(T)_2$와 고분자인 PeI-1T가 각각 1.80%, 4.06%의 효율을 나타내었다.

주요어: extended isoindigo, isoindigo, 전도성 단분자, 전도성 고분자, 유기태양전지, Knoevenagel condensation.
학번: 2013-23820